Journal of Applied Electrochemistry (2020) 50:501–511
https://doi.org/10.1007/s10800-020-01407-2

RESEARCH ARTICLE

Electrochemical synthesis of ZnO-WO_3 nanocomposites and their photocatalytic activity

Jenice Jean Goveas[1] · Sandhya Shetty[2] · Naveen Praveen Mascarenhas[1] · Renita Mishal D'Souza[1] · Richard Adolf Gonsalves[1]

Received: 23 September 2019 / Accepted: 3 February 2020 / Published online: 28 February 2020
© Springer Nature B.V. 2020

Abstract

Heterometal oxide nanoparticles of ZnO-WO_3 (ZWO) were synthesized using a facile dual step hybrid electrochemical–thermal technique. The role of surfactant additives during synthesis was investigated by introducing three different surfactants:Cetyltrimethyl ammonium bromide (Cetrimide), sodium dodecyl sulphate (SDS), and polyethylene glycol (PEG) into the electrolytic bath. X-ray diffraction and surface morphology studies indicate that the nanoparticles are cubic with an average crystallite size of 30–40 nm. Photocatalytic behaviour of these nanomaterials was tested using Methylene Blue (MB) and Eriochrome Black-T (EBT) as sample pollutants. The best results were observed for the photocatalyst generated in the presence of SDS as an additive and calcined at 650 ºC. High degree of decolourisation of both dyes resulting in complete mineralisation is due to the photocatalytic activity of ZWO which is greater than that of commercially obtained TiO_2-P25 photocatalysts. This proves that the electrochemical synthetic route with its low cost and high efficiency is an excellent technique for the bulk synthesis of heterometal oxide photocatalysts which could effectively be used in effluent water treatment.

Graphic Abstract

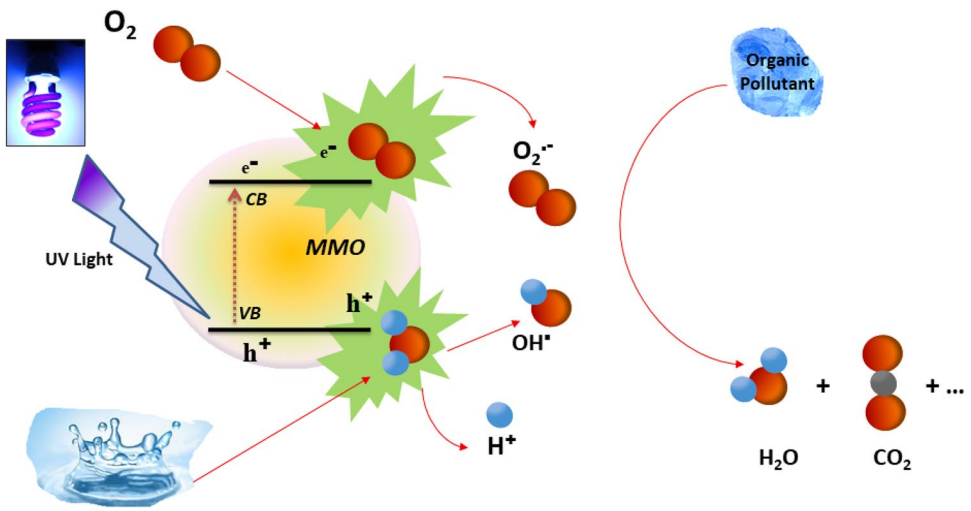

Keywords Heterometal oxide · Nanoparticles · Photocatalysis · Surfactant · Dye degradation

✉ Richard Adolf Gonsalves
richieag@yahoo.com

[1] Department of Chemistry, St. Aloysius College (Autonomous), Mangalore, Karnataka 575003, India

[2] Department of Chemistry, National Institute of Technology Karnataka, Srinivasnagar, Karnataka 575025, India

1 Introduction

Over the years semiconductor metal oxides have established themselves as very attractive photocatalysts especially for the photodegradation of organic waste and particularly dyes

in effluent water. They possess the advantage of bringing about complete mineralisation of these compounds [1, 2]. Photocatalytic degradation of organic dye effluents using nanostructured semiconductors is alluring and beneficial bearing in mind the affordability, ease of production, specificity and selectivity [3, 4]. They also possess relatively large turn-over capacity, retrievability and recyclability [5]. Semiconductor oxides of ZnO, WO_3, TiO_2, SnO_2, V_2O_5 and ZrO_2 have been found to be appealing photocatalysts as they possess good catalytic efficiency in degrading environmental pollutants like detergents, pesticides and dyes into simple molecules like carbon dioxide and water under UV light [6].

Zinc oxide is an important wide bandgap (3.34 eV) semiconducting transition metal oxide with promising features even at ambient temperature. It has good electron portability and luminescence coupled with large exciton binding energy (60 MeV) [7]. Furthermore, it is economical, has greater transparency and possesses more interstitial spaces and oxygen vacancies due to its wurtzite (hexagonal structure) and thus possesses oxygen binding and trapping ability [8]. Similarly, surface defects produce oxidative and catalytic properties and they become active sites for binding to polar substrates. In the presence of ultraviolet light, reactive oxygen species are generated on the surface which inhibit bacterial growth as well as degrade most of the persistent organic pollutants such as dyes [9, 10], pesticides and volatile organic compounds [11]. It has been favoured due to its ability to simultaneously bind to atomic oxygen and substrates for effective and dependable catalytic behaviour. Doping of ZnO NPs with other metal oxides might distort its crystal structure further, thereby improving its oxygen-retaining vacancies along with its substrate-binding ability. Such structural change may additionally improve the catalytic properties [12].

Tungsten is an important semiconductor which has gained increasing attention for its structural diversity and useful chemical and physical properties [10, 13], However, a serious limitation of pure tungsten metal oxide is its low quantum efficiency due to its high degree of e2 and hz recombination and also large band gap energy. Its quantum efficiency may be boosted by decreasing the probability of e2/hz recombination and decreasing the band gap energy [14]. These problems can be resolved when the pure metal oxide is replaced by composite materials especially with ZnO which shifts the absorption spectrum to the longer wavelength. This enables the possibility of using hetero-metal oxide nanoparticles of ZnO with oxides of another transition metal such as Tungsten.

Most of the methods adopted to synthesize metal oxide nanoparticles suffer from the requirements of expensive substrates, tedious procedures, sophisticated experiments, lengthier experimental duration and thorough experimental conditions [15]. This paper attempts to overcome those disadvantages by putting forward a unique facile electrochemical–thermal synthetic approach. The technique enables scalable production of photocatalytic mixed metal oxide nanoparticles of ZnO-WO_3 under ambient conditions. It is highly advantageous as it eliminates the need for using harsh chemicals making it a greener approach to satisfy the growing industrial demand for nanomaterials which can successfully degrade organic pollutants.

2 Materials and methods

Pure zinc metal plates (99.99%) were used for synthesis of nanoparticles. Sodium bicarbonate (AR grade: 99.5%) and Sodium tungstate (AR grade: 98.5%) were purchased from Sisco Research laboratories, Mumbai and Methylene Blue (MB) and Eriochrome Black-T (EBT) were purchased from S.D. Fine Chemicals Ltd, India. For the final preparation of the electrolyte solution, millipore water (specific resistance, 15 mΩ cm at 25 °C. Millipore Elix 3 water purification system, France) was used. A constant voltage of 12 V was supplied during electrolysis by a DC power supply (Model PS 618 potentiostat–galvanostat 302/2 A). Lastly, Whatman filter paper No. 41 was used during filtration process.

2.1 Synthesis of nanocomposites

A standard electrochemical technique was employed for the synthesis of the mixed metal oxide nanoparticles. Pure Zn plates were activated before electrolysis by dipping them in 0.1 M HCl for 30 s and rinsed with millipore water. 400 mL of a 0.02 M sodium salt solution of tungstate containing 0.01 moles of $NaHCO_3$ (added to increase the conductance) was taken in a pyrex vessel. The pH was maintained at 10 using NH_4OH/NH_4Cl buffer. Electrolysis was carried out in a rectangular undivided cell where pure Zn plates were used both as cathode and sacrificial anode. The electrolysis was carried out for about one hour under potentiostatic conditions at a potential of 12 V with constant stirring at 500 rpm. The white precipitate obtained was filtered, isolated from the solution and calcined in air at 2 different temperatures of 450 °C and 600 °C for an hour [16]. The synthesis was also repeated in the presence of 3 different surfactants: Cetrimide, SDS and PEG at concentrations of 3.88×10^{-3} M, 8.2×10^{-3} M and 8.04×10^{-5} M respectively which were added to the electrolytic bath in quantities just above their critical micellar concentration.

2.2 Assessment of photocatalytic activity of ZWO

Photocatalytic experiments were carried out in a 150×75 mm batch reactor. In order to evaluate the photocatalytic activity of the samples, photodegradation of MB and EBT

dye under UV light irradiation was carried out in the presence of ZWO nanoparticles at room temperature. The photochemical reactor used in this study was made of a Pyrex glass jacketed quartz tube. A high-pressure mercury vapor lamp (HPML) of 125 W (Philips, India) was placed inside the jacketed quartz tube at 30 ± 2 °C. A supply ballast and capacitor were connected in series with the lamp, in order to avoid fluctuations in the input light intensity. Water was circulated through the annulus of the quartz tube to evade heating of the solution. Reaction suspension was prepared by adding a catalytic load of 0.1 g of NPs in 100 mL of the dye solution (5, 10 and 25 ppm). Prior to illumination, the suspension was magnetically stirred for 2 h in dark to establish absorption–desorption equilibrium of the dye and also to ensure uniformity in the catalytic suspension. Subsequently, the dispersion containing dye and photocatalyst (ZWO) was irradiated under UV light. The lamp radiated predominantly at flux of 5.8×10^{-6} mol of photons s^{-1}. The dye-NP solution mixture was repeatedly illuminated for 10 min at 2 min intervals. During the 2 min interval, 3.0 mL of aliquots were taken from the test mixture. Because of progressive degradation of the dye with consecutive flashes, the intensity of the colour of the solution mixture decreased considerably. The change in colour of the dye solution as a function of time was monitored by using UV–Vis spectroscopy. The absorbance value of MB and EBT was taken at 660 nm and 568 nm, respectively. After each measurement, the aliquot along with the catalyst was transferred back to the reaction slurry to avoid volume and concentration change of both the dye and catalyst. The catalytic experiments were repeated thrice and the relative error was found to be less than ± 3.0%. The optimized photocatalyst was compared with the standard photocatalyst Degussa TiO_2-P25.

2.3 Catalyst characterization

Change in phase structure, crystallite size, surface morphology and chemical composition of the nanoparticles were evaluated using powder X-ray diffraction (XRD), transmission electron microscopy (TEM) and scanning electron microscopy (SEM). XRD data was recorded on Rigaku Miniflex 600 X-ray diffractometer with graphite monochromatized Cu-Ka (1.5406 Å) radiation, between the 2θ range from 10° to 90° at a scanning rate of 1° min^{-1}. The average crystallite sizes were estimated using Scherrer equation. The Fourier transform infrared spectrum (FTIR) of the sample was collected using Bruker Alpha-P spectrometer. The absorption spectrum of the sample was measured on a Shimadzu UV-1800 UV–Vis spectrophotometer. Surface morphology was observed by using SEM (EVO 18, Carl Zeiss, Germany). The composition of the coatings was studied by the energy dispersive X-ray (EDX) technique, interfaced with an SEM instrument. Structural analyses of the XRD patterns were conducted using computer software PANalytical X'Pert Highscore Plus. TEM images of the selected samples were recorded (Model: JEOL 2000 FX-II) with an acceleration voltage of 200 kV. 2 µL of ZnO-ethanol solution was dropped on a Cu grid with a carbon-reinforced plastic film.

3 Results and discussion

3.1 Compositional analysis of ZWO heterometal oxide nanostructures

XRD patterns of synthesized ZWO mixed metal oxide nanocomposites synthesized using SDS as an additive are represented in Fig. 1. The characteristic diffraction patterns of $ZnWO_4$, WO_3 and ZnO correspond to the monoclinic crystal phase and hexagonal wurtzite phase, respectively. The obtained diffraction peaks of $ZnWO_4$, WO_3 and ZnO match well with the JCPDS file no. 015-0774, 01-72-0677 and 01-089-0510, respectively [17]. No impurity peaks were observed. The result depicts the physical content homogenization which is further confirmed through SEM.

EDX is a well-established technique that enables precise determination of relative atomic concentration of different elements present in the nanocomposite [17]. EDX analysis of ZWO reveals the relative atomic abundance of zinc, tungsten and oxygen present in ZWO and other impurities were not observed. Semiquantitative analysis of the atomic concentration (atom %) is listed in Table 1.

EDX data as seen in Fig. 2 reveals that the ZWO Nanoparticles are composed of three elements which are Zn

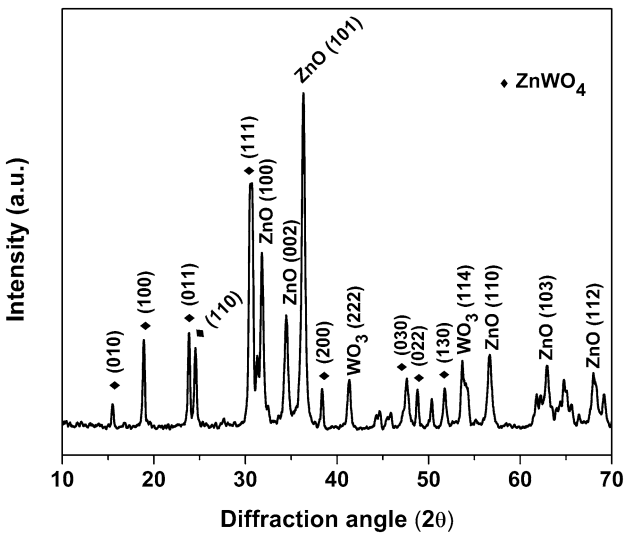

Fig. 1 XRD pattern of ZWO nanoparticles synthesized using SDS as additive

Table 1 Elemental composition of ZnO-WO_3 Nanoparticles synthesized under optimum conditions

Element	Weight%	Atomic%
Zn	62.672	46.36
W	27.605	7.21
O	15.448	46.42

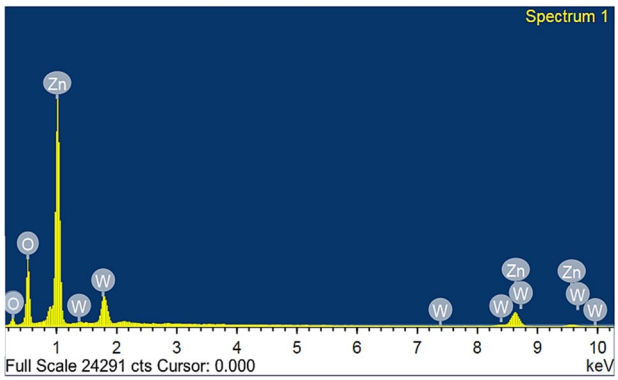

Fig. 2 EDX spectra of ZnO-WO_3 Nanoparticles synthesized under optimum conditions

(46.36%), Tungsten (7.21%) and O (46.42%). These results confirm the high purity of ZWO NPs.

3.2 Surface morphology studies

FESEM images show the role of the surfactant in changing the morphology of the NPs from nanoflakes-like less regular structures into more defined structures which act as better photocatalysts. Figure 3a shows the soft agglomeration of nanoparticles which reveals the cuboid morphology. The bundled agglomeration is a typical cluster of almost cuboidal structures which came together during calcination. The micrographs reveal that the morphology is replete possessing voids and pores. This may be attributed to the escape of gases during calcination. The crystallites are interlinked to each other forming a large network having irregular pore sizes.

TEM Analysis was carried out to understand the crystalline nature of ZWO nanoparticles. The images confirm that particles are almost spherical possessing non-uniform thickness.

It confirms the interactive mixing of ZnO and WO_3 particles which is essential for photocatalytic efficiency. Also, the particles are found to be embedded and attached to one another well, as seen from Fig. 4. This embedded system is a favourable accomplishment to achieve high degree of photochemical reaction. The average size of a primary particle is found to be 40 nm.

3.3 FTIR spectra

Figure 5 reveals the FTIR spectra of the ZWO NPs, collected from 400 to 4000 cm^{-1}. The bands observed in the range of 400 to 500 cm^{-1} typically correspond to the stretching vibration band for ZnO [18]. The absorption bands detected at 420, 444 and 477 cm^{-1} may be attributed to Zn-O bond stretching vibrations [19]. As observed in the Fig. 5b, ZnO absorption bands broadening is due to overlapping between the bands characteristic of WO_3 and ZnO [17]. An intense broad band observed at 3442 cm^{-1} is owing to W–OH stretching vibration and can be ascribed to intercalation of H_2O. A peak located at 1640 cm^{-1} is assigned to the W–OH bending vibration mode of the adsorbed molecules of water. The peak at 1402 cm^{-1} corresponds to W–O stretching

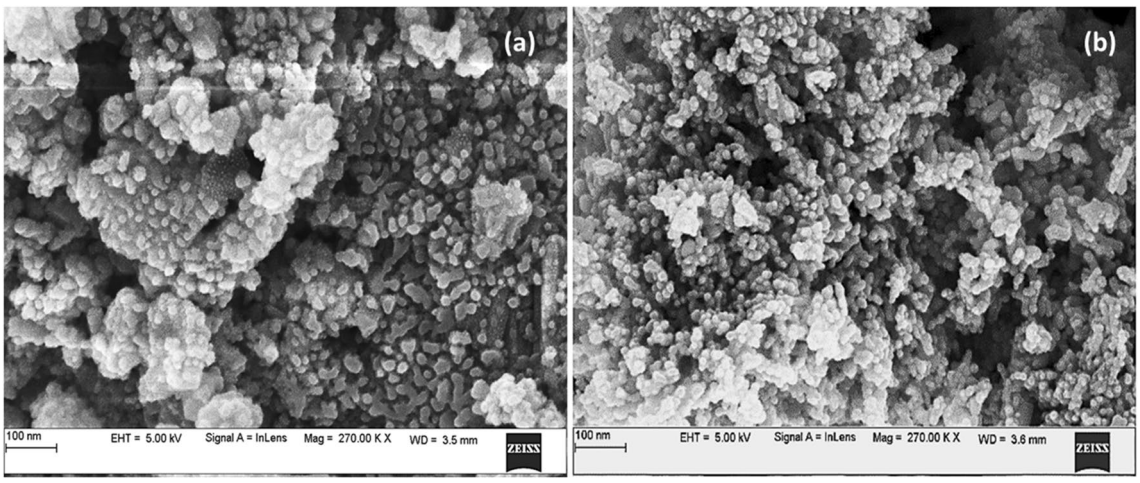

Fig. 3 SEM image of the electrochemically synthesized ZWO nanoparticles calcined at 650 °C **a** in the presence of SDS as additive **b** in the absence of surfactants

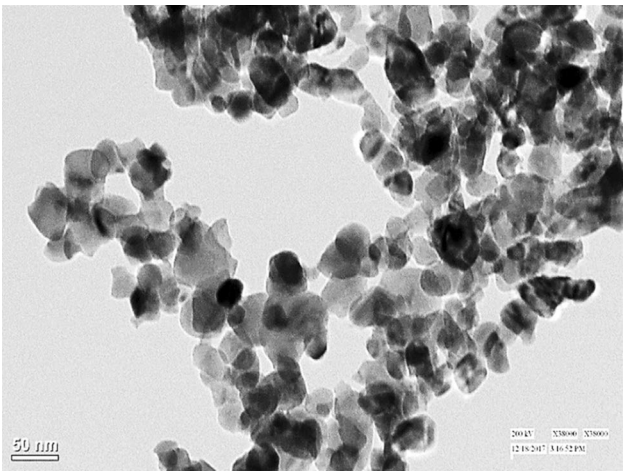

Fig. 4 TEM image of ZWO calcined at 650 °C synthesized using SDS as additive

vibration mode. Peaks are observed at 880 and 820 cm^{-1} which may be ascribed to the O–W–O stretching mode [20, 21].

3.4 UV–Vis diffuse reflectance spectra

Light absorption ability of ZWO semiconductor is studied by the band gap studies as depicted by the tauc plot in Fig. 6. Absorption bands showing broad tails were obtained between 380 to 500 nm for the particles. The bandgap for the nanocomposite is closer to ZnO giving a value of 2.84 eV. This is probably due to the formation of defect energy levels within the forbidden band.

3.5 Thermal stability assessment

Thermogravimetric analysis (TGA) reveals that the particles are highly stable to temperature (Fig. 7). Weight loss of 4.102% is observed at 900 °C which confirms the ability of the nanoparticles to withstand heat. Micro voids in the samples could be the reason to allow weight loss over 900 °C. Weight loss may also be due to thermal desorption of water and O_2 from the surface of ZWO particles. This indicates that nanopowders are pure and porous.

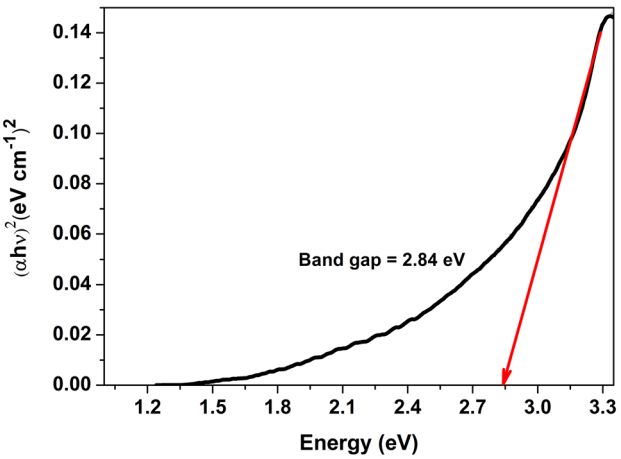

Fig. 6 Tauc Plot for band gap of ZWO calcined at 650 °C synthesized using SDS as additive

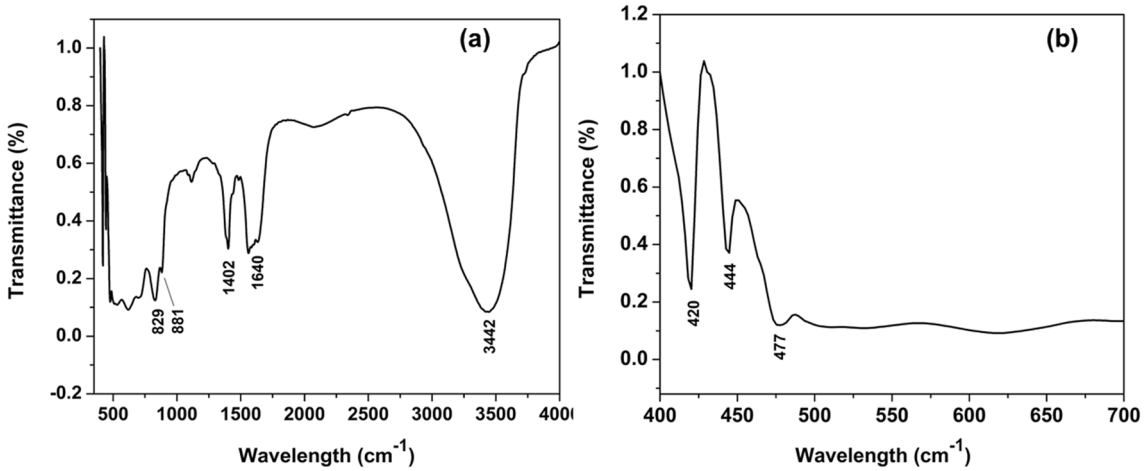

Fig. 5 FTIR spectra of ZWO **a** Synthesized using SDS as additive at 650 °C **b** Spectrum enlarged to reveal specific peaks between 400 and 500 cm^{-1}

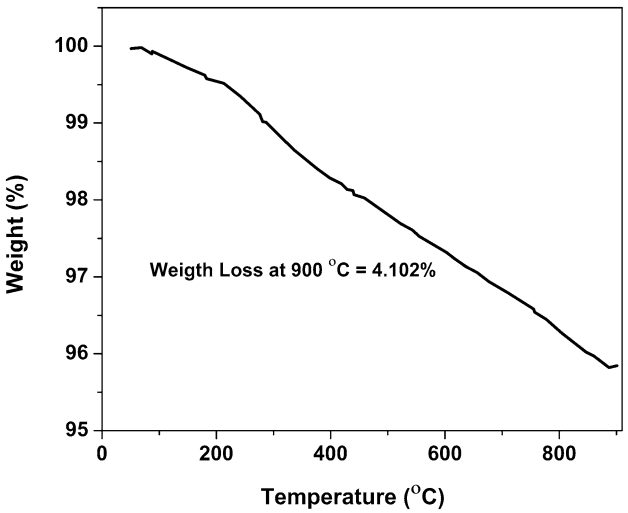

Fig. 7 TGA of ZWO nanoparticles synthesized at 650 °C using SDS as additive

3.6 Evaluation of photocatalytic activity

During photocatalysis, the dye solutions of MB and EBT along with the ZWO particles were kept in the dark with continuous stirring for 1 h in order to establish an adsorption equilibrium after which photocatalysis under UV light was carried on. Figure 8a and b respectively portray the relationship between photocatalytic ability of ZWO and irradiation time for different samples. For comparison sake, the commercially used very active Degussa P25 TiO_2 NPs were investigated under similar conditions. Blank degradation (in the absence of NPs) was carried out for background check which showed no significant degradation even after 1 h. When NPs were added to the solution in the presence of UV light, degradation took place and ZWO NPs displayed superior catalytic activity compared to P25 Degussa. It may be worth noting that ZWO NPs synthesized in the presence of SDS as surfactant and calcined at 650 °C

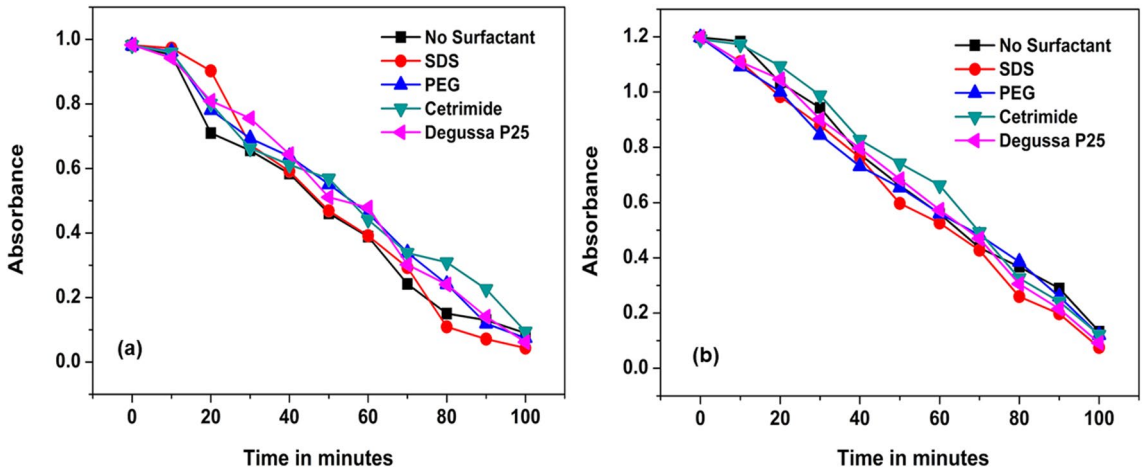

Fig. 8 Photocatalytic degradation of **a** MB and **b** EBT

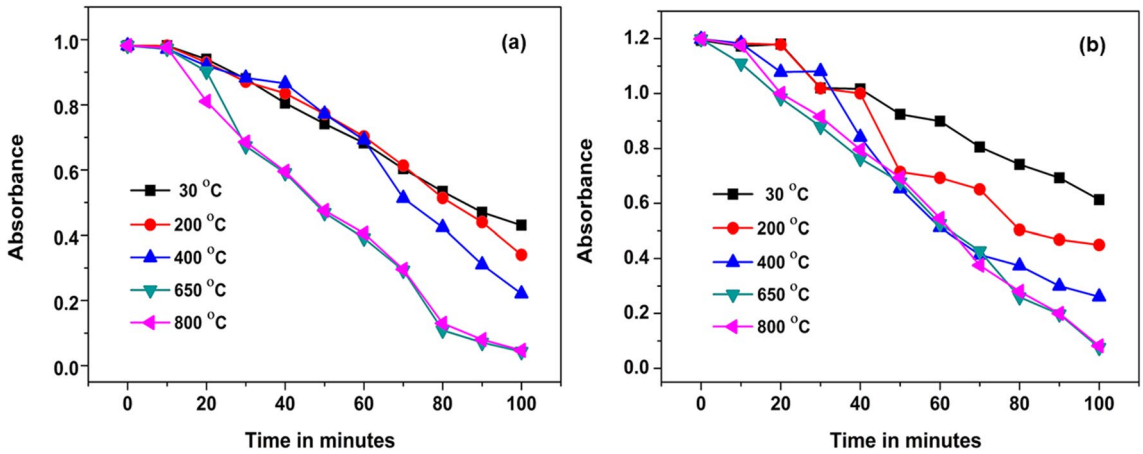

Fig. 9 Photocatalytic degradation of **a** MB and **b** EBT at different temperatures

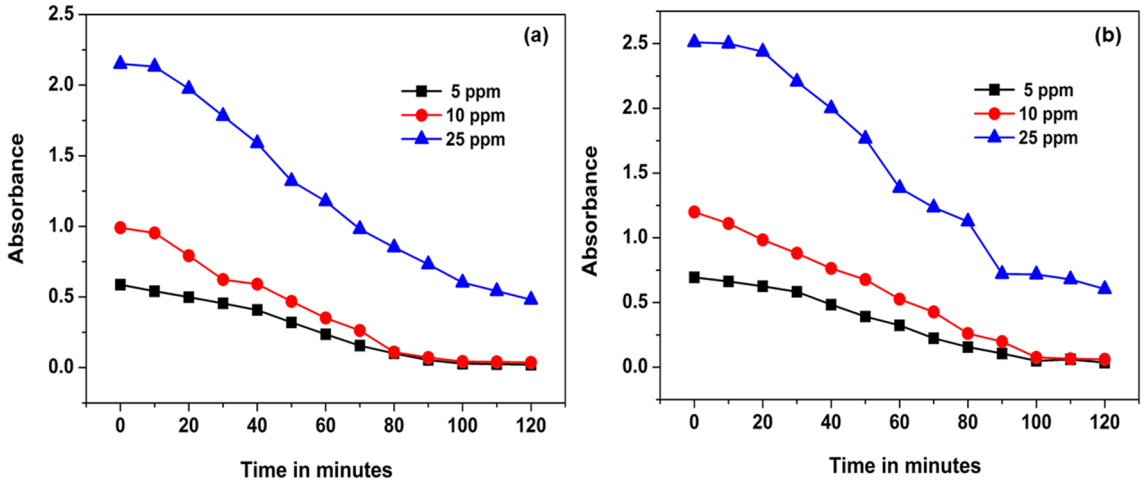

Fig. 10 Photocatalytic degradation using varying concentration of **a** MB **b** EBT

showed peak performance in degrading MBT and EBT to 95.6% and 93.7% within 100 min. This is significantly better than that of 92% which is reported for pure ZnO synthesized using a similar electrochemical method by Chandrappa et al. [22] and 90% reported for WO_3 thin films [23]. The enhancement of catalytic ability may be accredited to the development of defect energy levels inside the forbidden energy band of ZWO which decreases the band gap [24, 25] as discussed later. The percentage of degradation of the dye can be determined using the following formula % of degradation $= \frac{c_i - c_f}{c_i} \times 100$,where C_i and C_f are the initial and final dye concentrations respectively.

3.7 Effect of calcination temperature

The ZWO particles were synthesized using an electrochemical–thermal method and the effect of temperature of calcination on the nanocomposites synthesized is studied by assessing their photocatalytic ability. Particles synthesized at 30, 200, 400, 650 and 800 °C were used to degrade MB and EBT as represented in Fig. 9a and b respectively. In both cases it was observed that the photocatalytic property of the particles increased with increasing temperature of calcination till 650 °C after which the temperature did not play a major role in increasing the photocatalytic behaviour. Hence, 650 °C was taken as the optimum temperature for synthesis.

3.8 Effect of dye concentration

Degradation pattern for MB and EBT with three different concentrations of the dye 5 ppm, 10 ppm and 25 ppm are shown in Fig. 10a and b respectively. The nanoparticles showed most effective degradation for 10 ppm of the dye solution giving 95.6% and 93.7% degradation, respectively, for MB and EBT at 100 minutes of degradation time. For 25 ppm solutions of MB and EBT, 71.98% and 71.47% dye were degraded at the 100th minute, respectively. Hence, maximum efficiency was seen at 10 ppm concentration of the dye.

3.9 Kinetics of dye degradation

The photocatalytic action of the synthesized ZWO mixed oxide nanocomposites can be estimated using the kinetics of degradation of MB and EBT respectively. Photocatalysis is governed by the formula $-\ln C/C_0 = kt$ where C is the concentration of the dye at time t, C_0 is the initial concentration and k is the rate constant in min^{-1} [26].

Table 2 Kinetics parameters for the degradation of MB and EBT using different photocatalysts

Photocatalyst	MB		EBT	
	% Degradation	$k \times 10^{-2}$ min^{-1}	% Degradation	$k \times 10^{-2}$ min^{-1}
ZWO + no additive	90.8637	1.3621	88.9325	1.1906
ZWO + SDS	95.6003	1.7499	93.7010	1.4842
ZWO + PEG	92.4472	1.4798	89.9508	1.3409
ZWO + Cetrimide	90.4214	1.3694	89.7834	1.0978
Degussa P25 TiO_2	93.7328	1.3975	92.3616	1.3316

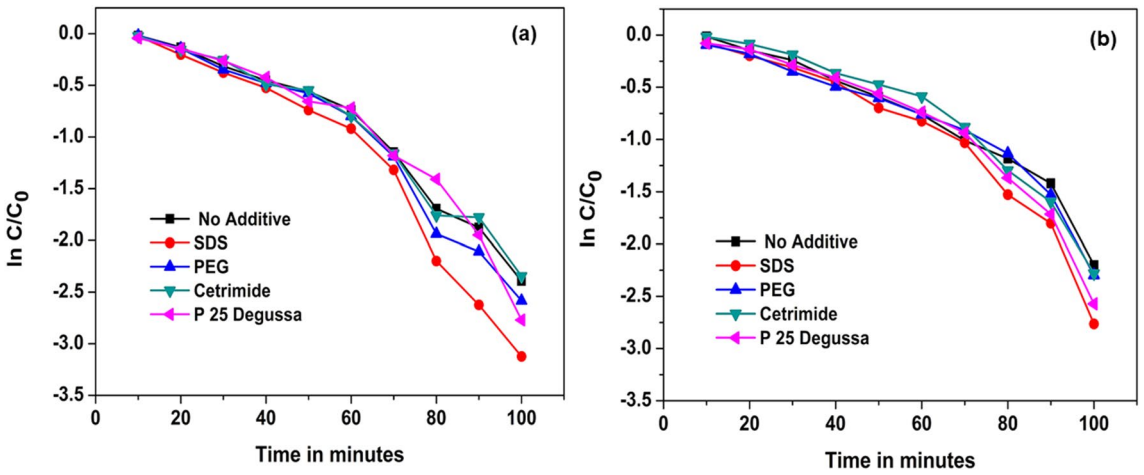

Fig. 11 Kinetic studies of the degradation of **a** MB and **b** EBT with different photocatalysts

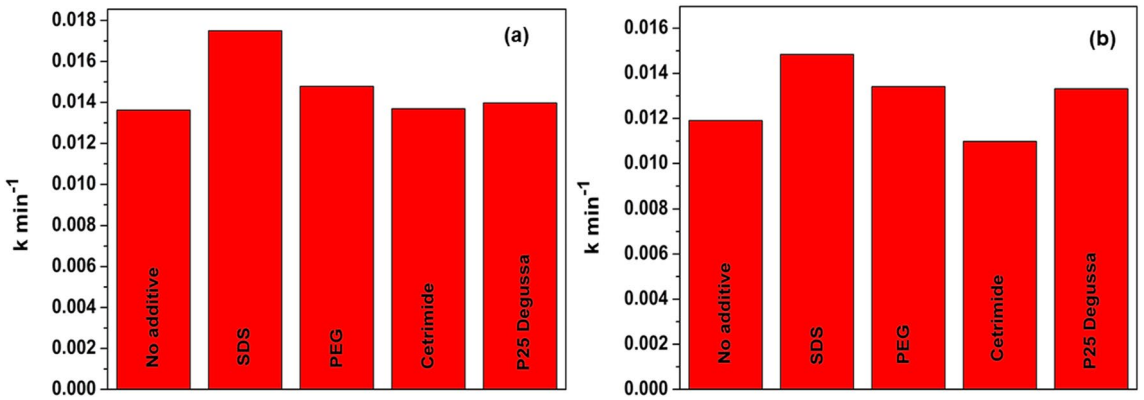

Fig. 12 Rate constant chart for the degradation of **a** MB and **b** EBT with different photocatalysts

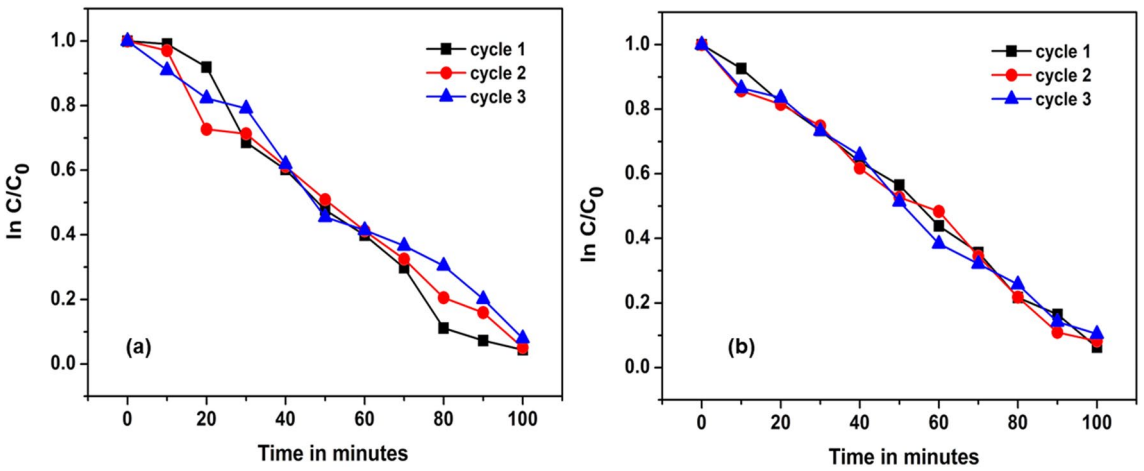

Fig. 13 Degradation profile of **a** MB and **b** EBT with the photocatalyst ZWO reused for three cycles

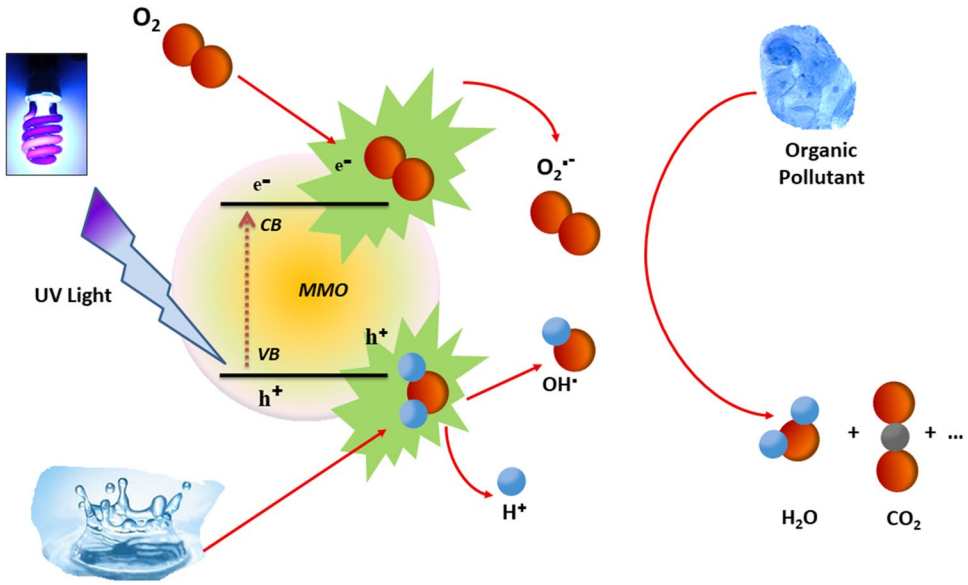

Fig. 14 Schematic diagram for the degradation of dye particles by ZWO nanoparticles

The obtained rate constants have been tabulated in Table 2. For comparison, P25 TiO_2 is used as a control under similar conditions. The table reveals that higher rate constants of 0.017499 min^{-1} and 0.014842 min^{-1} are obtained for ZWO synthesized using SDS as an additive. The reason for greater activity is probably due to the charge separation mechanism in the ZWO nanocomposite. The electron–hole combination reduces giving greater photocatalytic behaviour [27].

The kinetic plots of both MB and EBT synthesized without using surfactants and in the presence of SDS, PEG and Cetrimide is represented in Fig. 11a and b respectively. Photocatalytic degradation follows pseudo first order kinetics. The rate constant k (min^{-1}) for the different nanocomposites used for the photodegradation of MB and EBT have been calculated and represented in Fig. 12a and b respectively.

3.10 Reusability of the photocatalyst

Long-term use of the photocatalyst and its economic feasibility can be assessed by its reusability. The reusability of the optimum ZnO-WO_3 synthesized in the presence of SDS is described by the consecutive photocatalytic degradation efficiency for 10 ppm MB as shown in Fig. 13. The catalysts were centrifuged after every cycle and dried at 110 °C for the next cycle.

For each reusable experiment to be effective, proper adsorption–desorption equilibrium is first achieved. 95.6% MB degradation is achieved in the first run which decreases to 94.89% and 92.04% in the second and third run, respectively. Similarly, EBT degrades as 93.7%, 91.81% and 89.59% in first, second and third run, respectively. The decrease may be due to leaching of the photocatalyst surface which probably results in the loss of active sites. The various intermediaries formed due to the degradation of MB and EBT could also get adsorbed on the catalyst surface resulting in decreased efficiency of the photocatalyst.

The feasible energy storage mechanism in ZnO-WO_3 when irradiated under UV light is illustrated in Fig. 14. Enhanced photocatalytic activity of ZWO nanocomposite can be ascribed to the energy difference of WO_3 and ZnO which in turn decreases the band gap energy [28, 29]. Here, WO_3 behaves as the absorber owed to its absorption in the UV–Vis region, but its small band gap of 2.8 eV enables electron–hole pair recombination when coupled with ZnO [27]. On irradiation with UV light, activation of ZnO resulting in photogenerated electron–hole pairs is unlikely due to its large absorption gap. However, WO_3 with narrow band gap competently absorbs the UV light and gets excited generating electron–hole pairs [30]. These photogenerated electrons get transferred to the conduction band of ZnO reducing the likelihood for recombination of photogenerated electron–hole pairs. Thus, it increases the number of active species for degradation [31].

ZnO acts as co-catalyst that traps electron from further recombination. The photoelectrons effortlessly trap dissolved O_2 forming superoxide ($\cdot O_2^-$) anion radicals. Photoinduced holes trap OH^- to give ·OH radicals which bring about dye degradation [30]. The process is as follows [32, 33]:

Electron–hole pair generation:

$$WO_3 + h\nu \rightarrow WO_3\left(e^- - h^+\right),$$

$$ZnO + h\nu \rightarrow ZnO(e^- - h^+).$$

Charge transfer reaction:

$$\frac{WO_3\left(e^- - h^+\right)}{ZnO(e^- - h^+)} \rightarrow WO_3(e^-)/ZnO\left(h^+\right)$$

Radical formation:

$$WO_3(e^-) + O_2 \rightarrow WO_3 + O_2^-,$$

$$ZnO\left(h^+\right) + OH^- \rightarrow ZnO + OH.$$

Dye degradation

$$\text{Dye} + \frac{O_2^-}{OH\cdot} \rightarrow \text{Mineral acids} + CO_2 \uparrow + H_2O,$$

$$\text{Dye} + OH\cdot \rightarrow \text{Mineral acids} + CO_2 \uparrow + H_2O.$$

4 Conclusion

An efficient photocatalyst ZnO-WO_3 was synthesized using SDS as an additive by the electrochemical–thermal method calcined at 650 °C. These mixed metal oxide nanoparticles could bring about the successful photocatalytic decomposition of MB and EBT. WO_3 behaves as the absorber of light energy and ZnO acts as a co-catalyst which reduces the electron–hole recombination. The mixed metal oxide can be reused effectively though the degree of efficiency remains almost the same till three cycles and then decreases. Therefore, this study successfully demonstrates convenient utilization of the electrochemical–thermal route for the synthesis of ZnO-WO_3 nanoparticles which could be employed as effective photocatalysts and as plausible solutions to effluent water treatment.

Acknowledgements The authors are thankful to St. Aloysius College, Mangalore for providing laboratory facility to undertake this research. This research did not receive any specific grant from funding agencies in the public, commercial or not-for-profit sectors.

Compliance with ethical standards

Conflict of interest The authors declare that they have no conflict of interest.

References

1. Zheng Y, Zheng L, Zhan Y, Lin X, Zheng Q, Wei K (2007) Ag/ZnO heterostructure nanocrystals: synthesis, characterization, and photocatalysis. Inorg Chem 46(17):6980–6986
2. Colón G, Hidalgo M, Navío JA, Melián EP, Díaz OG, Dona J (2008) Influence of amine template on the photoactivity of TiO_2 nanoparticles obtained by hydrothermal treatment. Appl Catal B 78(1–2):176–182
3. Kim HG, Borse PH, Choi W, Lee JS (2005) Photocatalytic nanodiodes for visible-light photocatalysis. Angew Chem Int 44(29):4585–4589. https://doi.org/10.1002/anie.200500064
4. Marci G, Augugliaro V, López-Muñoz MJ, Martín C, Palmisano L, Rives V, Schiavello M, Tilley RJ, Venezia AM (2001) Preparation characterization and photocatalytic activity of polycrystalline ZnO/TiO_2 systems. 1. Surface and bulk characterization. J Phys Chem 105(5):1026–1032
5. An T-Q, Peng J-M, Tian Z-J, Zhao H-Y, Li N, Liu Y-M, Chen J-Z, Leng C-L, Sun Y, Chang D (2013) Pseudorabies virus variant in bartha-k61–vaccinated pigs, china, 2012. Emerg Infect Dis 19(11):1749–1755
6. Sehili T, Boule P, Lemaire J (1989) Photocatalysed transformation of chloroaromatic derivatives on zinc oxide II: Dichlorobenzenes. J Photochem Photobiol A 50(1):103–116
7. Jang YJ, Simer C, Ohm T (2006) Comparison of zinc oxide nanoparticles and its nano-crystalline particles on the photocatalytic degradation of methylene blue. Mater Res Bull 41(1):67–77
8. Bahşi ZB, Oral AY (2007) Effects of Mn and Cu doping on the microstructures and optical properties of sol–gel derived ZnO thin films. Opt Mater 29(6):672–678
9. Bautista P, Mohedano A, Casas J, Zazo J, Rodriguez J (2008) An overview of the application of Fenton oxidation to industrial wastewaters treatment. J Chem Technol Biotechnol 83(10):1323–1338
10. Xu A, Li X, Ye S, Yin G, Zeng Q (2011) Catalyzed oxidative degradation of methylene blue by in situ generated cobalt (II)-bicarbonate complexes with hydrogen peroxide. Appl Catal B 102(1–2):37–43
11. Rekha K, Nirmala M, Nair MG, Anukaliani A (2010) Structural, optical, photocatalytic and antibacterial activity of zinc oxide and manganese doped zinc oxide nanoparticles. Physica B 405(15):3180–3185
12. Chandrappa KG, Venkatesha TV, Vathsala K, Shivakumara C (2010) A hybrid electrochemical–thermal method for the preparation of large ZnO nanoparticles. J Nanopart Res 12(7):2667–2678
13. Santos L, Silveira CM, Elangovan E, Neto JP, Nunes D, Pereira L, Martins R, Viegas J, Moura JJ, Todorovic S (2016) Synthesis of WO_3 nanoparticles for biosensing applications. Sens Actuators B 223:186–194
14. binti Harun NFA, bin Mohd Y, Pei LY, Chin LY (2018) Fabrication of tungsten trioxide-loaded titania nanotubes as a potential photoanode for photoelectrochemical cell. Int J Electrochem Sci 13:5041–5053
15. Reddy VR, Manjunath V, Janardhanam V, Kil Y-H, Choi C-J (2014) Electrical properties and current transport mechanisms of the Au/*n*-GaN Schottky structure with solution-processed high-k $BaTiO_3$ interlayer. J Electron Mater 43(9):3499–3507
16. Goveas JJ, Shetty S, Mascarenhas NP, Hegde AC, Gonsalves RA (2018) Corrosion inhibiting action of Ni–Mo alloy coatings in the presence of mixed metal oxide nanocomposites. New J Chem 42(16):13660–13666
17. Xie J, Zhou Z, Lian Y, Hao Y, Liu X, Li M, Wei Y (2014) Simple preparation of WO_3–ZnO composites with UV–Vis photocatalytic activity and energy storage ability. Ceram Int 40(8):12519–12524
18. Gholami M, Shirzad-Siboni M, Farzadkia M, Yang J-K (2016) Synthesis, characterization, and application of ZnO/TiO_2 nanocomposite for photocatalysis of a herbicide (Bentazon). Desalin Water Treat 57(29):13632–13644
19. Gonçalves P, Bertholdo R, Dias JA, Maestrelli SC, Giraldi TR (2017) Evaluation of the photocatalytic potential of TiO_2 and ZnO obtained by different wet chemical methods. Mater Res 20:181–189

20. Ghosh S, Acharyya SS, Kumar M, Bal R (2015) One-pot preparation of nanocrystalline Ag-WO_3 catalyst for the selective oxidation of styrene. RSC Adv 5(47):37610–37616
21. Shen Y, Wang W, Chen X, Zhang B, Wei D, Gao S, Cui B (2016) Nitrogen dioxide sensing using tungsten oxide microspheres with hierarchical nanorod-assembled architectures by a complexing surfactant-mediated hydrothermal route. J Mater Chem A 4(4):1345–1352
22. Chandrappa KG, Venkatesha TV (2012) Electrochemical synthesis and photocatalytic property of zinc oxide nanoparticles. Nano-Micro Lett 4(1):14–24
23. Dong P, Yang B, Liu C, Xu F, Xi X, Hou G, Shao R (2017) Highly enhanced photocatalytic activity of WO_3 thin films loaded with Pt–Ag bimetallic alloy nanoparticles. RSC Adv 7(2):947–956
24. Chai SY, Kim YJ, Lee WI (2006) Photocatalytic WO_3/TiO_2 nanoparticles working under visible light. J Electroceram 17(2–4):909–912
25. Higashimoto S, Ushiroda Y, Azuma M (2008) Electrochemically assisted photocatalysis of hybrid WO_3/TiO_2 films: effect of the WO_3 structures on charge separation behavior. Top Catal 47(3–4):148–154
26. Yin R, Luo Q, Wang D, Sun H, Li Y, Li X, An J (2014) SnO_2/gC_3N_4 photocatalyst with enhanced visible-light photocatalytic activity. J Mater Sci 49(17):6067–6073
27. Adhikari S, Sarkar D, Madras G (2015) Highly efficient WO_3–ZnO mixed oxides for photocatalysis. RSC Adv 5(16):11895–11904
28. Changlin Y, Kai Y, Qing S, Jimmy CY, Fangfang C, Xin L (2011) Preparation of WO_3/ZnO composite photocatalyst and its photocatalytic performance. Chin J Catal 32(3–4):555–565
29. Shifu C, Lei C, Shen G, Gengyu C (2005) The preparation of coupled WO_3/TiO_2 photocatalyst by ball milling. Powder Technol 160(3):198–202
30. Yang Y, Zhang T, Le L, Ruan X, Fang P, Pan C, Xiong R, Shi J, Wei J (2014) Quick and facile preparation of visible light-driven TiO_2 photocatalyst with high absorption and photocatalytic activity. Sci Rep 4:7045
31. Ameta S, Ameta R (2018) Advanced oxidation processes for wastewater treatment: emerging green chemical technology. Academic Press, London
32. Nosaka Y, Nosaka A (2016) Understanding hydroxyl radical (•OH) generation processes in photocatalysis. ACS Energy Lett 1(2):356–359
33. Godin R, Hisatomi T, Domen K, Durrant JR (2018) Understanding the visible-light photocatalytic activity of GaN: ZnO solid solution: the role of Rh_2-y$CryO_3$ cocatalyst and charge carrier lifetimes over tens of seconds. Chem Sci 9:7546–7555

Publisher's Note Springer Nature remains neutral with regard to jurisdictional claims in published maps and institutional affiliations.